# ChemInform Abstract: Properties of the HCl/Ice, HBr/Ice, and H2O/Ice Interface at Stratospheric Temperatures (200 K) and Its Importance for Atmospheric Heterogeneous Reactions

**ARTICLE** *in* CHEMINFORM · FEBRUARY 2001

Impact Factor: 0.74 · DOI: 10.1002/chin.200108014



**3 AUTHORS**, INCLUDING:

Michel J Rossi
Paul Scherrer Institut
**259** PUBLICATIONS **6,466** CITATIONS

# Properties of the HCl/Ice, HBr/Ice, and $H_2O$/Ice Interface at Stratospheric Temperatures (200 K) and Its Importance for Atmospheric Heterogeneous Reactions

**Benoît Fluckiger, Laurent Chaix,† and Michel J. Rossi***

*Laboratory of Air Pollution Studies (LPA), Département de Génie Rural (DGR), Swiss Federal Institute of Technology (EPFL), CH-1015 Lausanne, Switzerland*

*Received: January 21, 2000; In Final Form: August 14, 2000*

The properties of the interface region of bulk, vapor-deposited, and single-crystal ice have been studied in a Knudsen cell flow reactor in the range 190−210 K using repetitive pulse experiments (RPEs) at variable frequency. Fluxes of surface-to-bulk loss in ice on single-crystal and bulk ice vary from $5 \times 10^{11}$ to $1 \times 10^{13}$ and from $5 \times 10^{12}$ to $5 \times 10^{14}$ molecule $s^{-1}$ $cm^{-2}$ for HCl and $D_2O$, respectively. A positive activation energy for diffusional loss of $E_A = 3.0 \pm 0.5$ kcal/mol for HCl/ice and $5.3 \pm 0.7$ kcal/mol for $D_2O$/ice has been measured. Complementary measurements ("dope and probe" experiments) of the HCl/ice interface region using the titration reaction of $ClONO_2 + HCl \rightarrow Cl_2 + HNO_3$ are in good agreement with the diffusional loss measurements from RPEs. These experiments allowed the evaluation of the thickness $h$ of the interfacial region, defined as the near-surface region of the ice where HCl is immediately available for titration at a high rate. We measured $h = 100 \pm 10$ nm for single-crystal ice, $200 \pm 50$ nm for vapor-deposited ice, and $1000 \pm 200$ nm for bulk ice samples. The modeling of our results according to the laws of diffusion leads to values of the HCl diffusion coefficient $D_{HCl}$ ranging from $(4.0 \pm 1.0) \times 10^{-14}$ to $(2.8 \pm 1.0) \times 10^{-12}$ $cm^2$ $s^{-1}$ for single-crystal and bulk ice, respectively.

## Introduction

Heterogeneous chemistry plays an important role in the atmosphere. The composition of the stratosphere can be affected by heterogeneous reactions on atmospheric particulate or aerosols. The seasonal formation of the Antarctic ozone hole[1,2] is a dramatic example of surface chemistry occurring on polar stratospheric clouds (PSCs) following reactions R-1, R-2, and R-3, which convert inactive chlorine in the form of reservoir molecules such as $ClONO_2$ and HCl into a photolabile form such as $Cl_2$ and HOCl at the interface of frozen particulates.

$$ClONO_2(g) + HCl(s) \xrightarrow{k_1} Cl_2(g) + HNO_3(s) \quad \text{(R-1)}$$

$$ClONO_2(g) + H_2O(s) \xrightarrow{k_2} HOCl(g) + HNO_3(s) \quad \text{(R-2)}$$

$$HOCl(g) + HCl(s) \xrightarrow{k_3} Cl_2(g) + H_2O(s) \quad \text{(R-3)}$$

By production of condensed-phase $HNO_3$, reactions R-1 and R-2 remove the principal component of $NO_y$ from the gas phase, similar to the hydrolysis of $N_2O_5$ on frozen particles. As a result, less $NO_2$ is available to deactivate ClO to $ClONO_2$ and ozone loss is prolonged. The formation of condensed-phase products such as $H_2O/HNO_3$ mixtures at the interface of ice[3] could affect further uptake of reactants; Hanson and Ravishankara[4] measured an uptake coefficient $\gamma$ of 0.006 for the heterogeneous reaction R-2 of $ClONO_2$ on nitric acid trihydrate (NAT) at 201 K, which is approximately 2 orders of magnitude slower than the corresponding reaction on a pure ice surface.

Chlorine nitrate interacting with frozen particles (PSC I and II, saturated ternary solutions) undergoes the competing reactions R-1 and R-2. The properties of the interfacial region, defined in our study as the near-surface region of the frozen particles in which adsorbed species such as HCl are able to directly interact with $ClONO_2$ without delay, are deemed to be important in order to establish the branching ratio between hydrolysis (R-2) and halogen exchange (R-1). The total uptake of HCl on ice and its availability for bimolecular reactions were found to depend on the surface area of the ice.[5]

Experimental studies of heterogeneous chemistry have to date used techniques taken from either gas kinetics or classical surface science to probe the effects of exposing thin films of ice and acid hydrates to atmospheric gases of interest. Although the probe techniques used so far (reflection−absorption IR spectroscopy (RAIRS), attenuated total reflection (ATR) spectroscopy , flow tubes, Knudsen cells, etc.[6]) have proved to be extremely effective, they are in general sensitive only to specific aspects of a given reaction. When considering the kinetics of heterogeneous atmospheric reactions, the interplay of processes such as adsorption, desorption, and diffusion in/on the condensed phase needs to be properly understood. These processes may be expected to vary considerably in their relative importance as composition and temperature change. The presence of particles in the atmosphere in which the adsorbates or reaction products may be soluble increases the importance of surface-to-bulk exchange processes in heterogeneous atmospheric chemistry. In solid atmospheric particles, the rates of diffusion away from the surface into the bulk are likely to be significantly slower than those for liquid droplets. Nevertheless, surface-to-bulk diffusion is still likely to be an important route for surface regeneration on atmospheric time scales when molecular mobilities are sufficiently high. The study of bulk diffusion in atmospheric solids is a challenge using existing techniques,

* To whom correspondence should be addressed.
† Present address: Ecrins Automatishes 98, Rue du Pré de l'Homme F-38920 Crolles, France.

10.1021/jp000273g CCC: $19.00 
Published on Web 11/22/2000

**TABLE 1: Characteristic Parameters and Relevant Kinetic Expressions**

| | |
|---|---|
| reactor volume $V$ | 2000 $cm^3$ |
| estimated internal reactor surface area $A_R$ | 1300 $cm^2$ |
| sample geometric surface area $A_S$ | 15 $cm^2$ |
| gas number density $N = F/(Vk_{esc})$[a] | $(1-1000) \times 10^{10}$ $cm^{-3}$ |
| escape rate constant (expt) | $k_{esc}(ClONO_2) = 3.0 \pm 0.3$ $s^{-1}$ (Ø 14 mm aperture) |
| | $k_{esc}(HCl) = 0.66 \pm 0.05$ $s^{-1}$ (Ø 4 mm aperture) |
| | $k_{esc}(H_2O) = 0.93 \pm 0.05$ $s^{-1}$ (Ø 4 mm aperture) |
| first-order rate constant $k_{uni}$ [$s^{-1}$] | $k_{uni} = [(S^i/S^o) - 1]k_{esc}$[b] |
| collision frequency $\omega$ [$s^{-1}$] | $\omega = (\langle c \rangle/4V)A_s$ = 47.6 for $ClONO_2$[c] |
| uptake coefficient $\gamma$ | $\gamma = k_{uni}/\omega$ |

[a] $F$ = flow into the reactor [molecule $s^{-1}$]. [b] $S^i$ and $S^o$ are the initial and steady-state MS signals, respectively. [c] $\langle c \rangle$ = mean molecular speed.

which are largely unable to focus upon specific regions of the mimicking films they probe. However, some progress has been made recently in this area by Vickerman and Donsig using secondary ion mass spectrometry (SIMS) to establish depth profiles in ice films which have been exposed to chlorine-containing molecules.[7,8]

We present *rate* measurements of HCl, $D_2O$, and HBr concerned with surface-to-bulk processes on different types of ice. The comparison of the time dependence of the interaction of these three gaseous species with the ice substrate revealed a slow loss process, which occurs on a much longer time scale compared to adsorption and desorption. This additional sink for the gas phase was attributed to the removal of a fraction of the adsorbed species at the interface into the bulk, which is characterized in this work by the flux of surface-to-bulk loss $F_L$ of adsorbed HCl, $D_2O$, and HBr. "Dope and probe" experiments using the titration reaction R-1 of $ClONO_2$ with HCl permitted correlation of the flux of surface-to-bulk loss with the condensed-phase (bulk) diffusion coefficient $D_{HCl}$ according to the laws of diffusion. Parameters of the interfacial region such as its thickness $h$ and the HCl mole fraction are assessed as a corollary. Finally, we compare the values of $D_{HCl}$ with literature values.

## Experimental Setup

The experiments were performed in a Teflon-coated Knudsen flow reactor operating in the molecular flow regime. This technique has been described in sufficient detail in the literature.[9] Briefly, the gases under study were introduced into the Knudsen reactor from the gas-handling system by using either a capillary for pressure reduction or a pulsed valve as a flow-controlling device. The gases leave the Knudsen reactor through an escape orifice whose diameter (14 mm) determines the residence time and the concentration inside the Knudsen reactor. The characteristic parameters of the reactor are given in Table 1. The modulated effusive beam leaving the Knudsen cell is analyzed by a quadrupole mass spectrometer (MS) whose settings were chosen to yield a sensitivity of approximately $10^{10}$ molecules $cm^{-3}$ at a signal-to-noise ratio >2.

An isolation plunger allows the separation of the reactive surface located in the sample chamber from the reactor volume. Pulsed valve experiments are performed by introducing a known dose in the range of $10^{14}-10^{16}$ molecules into the reactor across a solenoid valve at a pulse duration of a few milliseconds. The observed single-exponential decay in the presence of a reactive surface is characterized by a rate constant which is the sum of

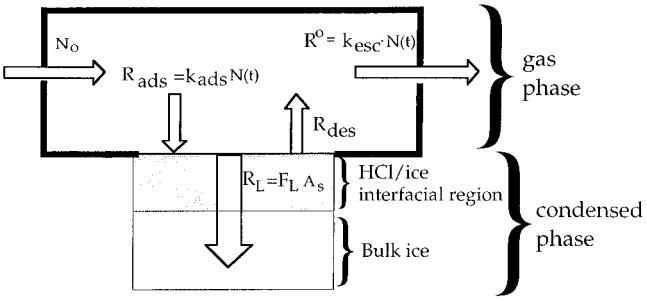


**Figure 1.** Schematic view of the relevant rate processes occurring in the flow reactor during a reactive experiment: $N_0$ is the injected dose; $R_0 = k_{esc}N(t)$ is the flow rate effusing out of the reactor; $k_{ads}N(t)$ and $R_{des}$ are the rates of adsorption and desorption [molecules $s^{-1}$], respectively; $R_L$ [molecule $s^{-1}$] is the rate of surface-to-bulk loss with $F_L$ being the corresponding flux [molecule $s^{-1}$ $cm^{-2}$].

the escape rate constant $k_{esc}$ and the pseudo-first-order reaction rate constant, namely, $k_{uni}$ (Table 1). The rate constant for effusive loss $k_{esc}$ is determined by fitting an exponential decay function to the experimental MS signal trace in the absence of reaction. The second type of experiments is continuous flow or steady-state experiments which are performed by introducing a constant flow of molecules across a capillary into the flow reactor. The change of the MS signal levels of the corresponding compounds upon opening ($S^o$) and closing ($S^i$) the sample chamber obtains a value for the net uptake coefficient $\gamma$ (Table 1). In addition, steady-state experiments allow the establishment of a mass balance between reactants consumed and products formed during the reaction. We used a low-temperature sample support in which the sample could be cooled to 150 K. A programmable temperature controller maintained the final temperature to $\pm 0.5$ K at an accuracy of $\pm 2$ K.[9]

## Preparation of the Ice Samples

For the preparation of bulk ice (B) samples, approximately 5 mL of degassed distilled water was poured into the sample support at ambient temperature, cooled to the desired temperature in about 15 min, and subsequently evacuated. For single-crystal ice (SC) preparation, the cooling was much slower ($-0.3$ K $min^{-1}$) in the temperature range of 0 to $-30$ °C following a procedure of Knight et al.[10] in order to avoid possible supercooling of the water. The SC sample we obtained appeared more transparent than B samples. We do not have at present an optical characterization for pure single-crystal ice, but we noticed that this preparation procedure led to ice samples which clearly influenced our results. In addition, SC ice has distinctly different kinetics of $H_2O$ condensation and evaporation in relation to B samples.[11] For condensed ice (C), the mounted and evacuated sample support was cooled to the desired temperature of typically 200 K, followed by condensation of water from the gas phase at a flow rate of $F = 10^{18}$ molecule/s. The calculated thickness using the known density of ice of 0.92 g $cm^{-3}$ for low-temperature C samples was in the range of $2-10$ $\mu$m. All experiments presented in this work have been performed on "desorbing" ice samples, that is, without adding an external flow of $H_2O$ vapor which usually compensates for the rate of $H_2O$ evaporation off the ice sample.

## Description of the Measurement of the Flux of Surface-to-Bulk Loss ($F_L$) in Repetitive Pulse Experiments (RPEs)

We explain below the meaning of the term surface-to-bulk loss ($F_L$) and its measurement using RPEs. Figure 1 shows the

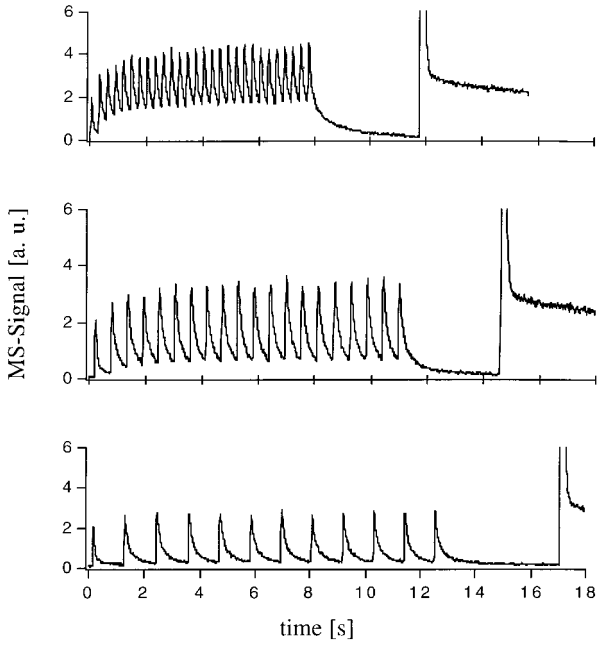


**Figure 2.** Raw data of RPEs of HCl interacting with ice at 190 K. The time intervals between each pulse are 0.3 s (upper trace), 0.6 s (middle trace), and 1.12 s (lower trace). The dose per pulse corresponds to approximately $2 \times 10^{14}$ molecules with a pulse duration set to 1 ms. Each trace is terminated by a large reactive pulse of $5 \times 10^{15}$ molecules, leading to an equilibrium HCl vapor pressure at steady-state conditions. The pulse trains correspond to the following cumulative doses: upper, $1.7 \times 10^{16}$ molecules; middle, $1.2 \times 10^{16}$ molecules; lower, $7.2 \times 10^{15}$ molecules.

main rate processes occurring in the reactor when a pulse of $N_0$ molecules interacts with an ice sample. The MS signal is proportional to the time-dependent flow rate $R_0 = k_{esc} N(t)$ effusing out of the reactor. $N(t)$ is the total number of molecules at time $t$ and $N(t=0) = N_0$. The heterogeneous processes are characterized by the rate of adsorption $R_{ads} = k_{ads} N(t)$, the rate of desorption $R_{des}$, and the rate of surface-to-bulk loss $R_L = F_L A_s$ with $F_L$ being the flux. We stress that the time scale for $R_L$ is much longer compared to $R_{ads}$ and $R_{des}$; the HCl molecules taken up on the ice sample which have not desorbed during the gas-phase residence time $\tau = 1/k_{esc}$ continue to disappear from the interface into the bulk, even at vanishing HCl concentration in the gas phase.

Figure 2 displays results of typical RPEs of HCl interacting with an ice substrate performed at three injection frequencies ranging from 0.5 (lower trace) to 3.5 Hz (upper trace). The individual dose per pulse within each pulse train is $\sim 6 \times 10^{14}$ molecules, whereas the large ("giant") pulse displayed at the right-hand side of Figure 2 approximately corresponds to $5 \times 10^{15}$ molecules or roughly one-half of a molecular monolayer. Thus the cumulative dose of the upper, middle, and lower pulse trains in Figure 2 corresponds to 3.4, 2.4, and 1.4 times the dose dispensed in the "giant" pulse displayed on the right, respectively (see Figure 2). The HCl partial pressures $P_{HCl}$ obtained after each individual pulse within a pulse train are distinctly lower than those of the quasi-steady-state level obtained after the admission of the giant single pulse which corresponds to the vapor pressure above a liquid HCl/$H_2O$ solution atop the ice substrate. This latter HCl vapor pressure is given by the liquid/solid coexistence line in the HCl/$H_2O$ phase diagram.[12]

Figure 3 displays the integral of both the reference pulse corresponding to the integral dose of HCl dispensed and the

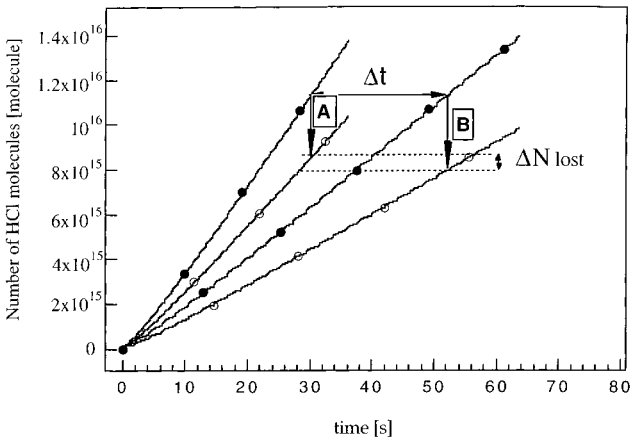


**Figure 3.** Integrated HCl flows in RPEs as a function of time. The lines labeled with full circles are the reference series at injection frequencies of 3 and 1.7 Hz, respectively. The lines labeled with open circles are the corresponding reactive traces. The same cumulative dose is reached, for example, at $t_1 = 30$ s and $t_2 = 52$ s, respectively. The ratio $\Delta N_{lost}/\Delta t$ represents the rate of surface-to-bulk loss, $R_L$.

train of sample pulses such as displayed in Figure 2 corresponding to the total number of HCl molecules effusing out of the flow reactor and thus not retained by the ice substrate. The difference of two integrals, such as $A$ and $B$ of Figure 3, at a given time $t$ after the start of a RPE is equivalent to the number $N_{lost}(t)$ of HCl taken up by the ice substrate at $t$, where $N_{lost}(t_1) = A$ and $N_{lost}(t_2) = B$. We now compare two values $N_{lost}(t)$ obtained at two injection frequencies $f_1$ and $f_2$ ($f_1 > f_2$) under the constraint $t_1 f_1 = t_2 f_2$, that is, at an equal applied dose of HCl. This constraint corresponds to applying a horizontal cut to the line labeled $\Delta t$ in Figure 3. Because $f_1 > f_2$, we obtain $t_1 < t_2$ such that the time $t_2$ elapsed after the RPE performed at $f_2$ is longer than $t_1$ for RPE ($f_1$). We now consider the difference $\Delta N_{lost}(t) = N_{lost}(t_2) - N_{lost}(t_1)$ under the above constraint $t_1 f_1 = t_2 f_2$ and find $N_{lost}(t_2) = B > N_{lost}(t_1) = A$. We interpret $\Delta N_{lost}(t)$ as a loss of HCl owing to diffusion of HCl from the interface region into the bulk of the ice substrate whose rate $R_L$ is given by $(N_{lost}(t_2) - N_{lost}(t_1))/\Delta t$.[13] It is important to note that every change in the experimental parameters of the HCl-dosing such as pulse frequency or pulse amplitude is reflected in the experimental data as far as adsorption and desorption processes are included because the signal displayed in Figure 3 (reactive traces, open circles) represents the net effect. $\Delta N_{lost}(t)$ displayed in Figure 3 therefore corresponds to the difference of total molecules lost from the gas phase other than by adsorption and effusion of HCl.

We emphasize that for the time being the rate law of $R_L$ has not yet been shown to follow Fick's law of diffusion and that it is obtained as a difference of two loss processes of gas-phase HCl. Note that the MS signal decreases to zero in a single-exponential manner with a decay constant $k_{ads}$ after the last individual pulse of each pulse train (see Figure 2). This behavior is in stark contrast to that of the steady-state level which spontaneously forms after admission of the giant pulse (right-hand side of Figure 2) even though the cumulative dose dispensed during the RPE has been larger than the single dose of $5 \times 10^{15}$ molecules. The difference between the two cases, namely sequential and single pulse injection, arises from the fact that HCl adsorbed during the RPE has had ample time to diffuse into the bulk so that it becomes unavailable to sustain the steady-state level shown on the right-hand side of Figure 2. We take this observation as an indication of the loss of HCl into the bulk on the time scale of the RPE.

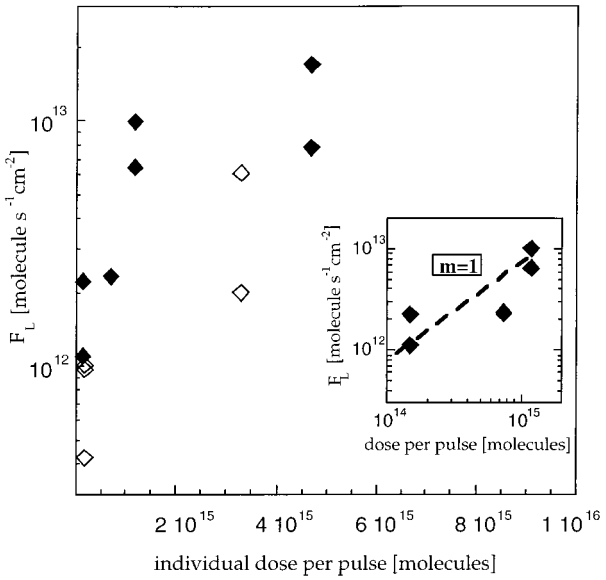


**Figure 4.** Flux $F_L$ of HCl surface-to-bulk loss at 200 K on bulk ice (B) (♦) and single-crystal ice (SC) (◇), as a function of the individual dose per pulse. The inset displays the first-order dependence of $F_L$ on the dose up to $2 \times 10^{15}$ molecules per pulse ($m = 1$).

### Results of Repetitive Pulse Experiments

**Influence of the Type of Substrate on the Diffusive Loss of HCl, HBr, and $D_2O$.** *$F_L$ for HCl on Bulk (B) and Single-Crystal Ice (SC) in the Temperature Range of 190−210 K.* Figure 4 displays the flux of HCl surface-to-bulk loss $F_L$ according to the above procedure on bulk (B) and single-crystal ice (SC) samples at 200 K as a function of the individual HCl dose of a RPE. The $F_L$ values are independent of the pair of injection frequencies within experimental error, in the range of 0.3−3.5 Hz which is the highest RPE frequency we used. The upper limit of 3.5 Hz approximately corresponds to the escape rate constant $k_{esc}$ for HCl; this upper limit ensures that the identity of the individual pulses is maintained during the RPE. The values of $F_L$ range from $5 \times 10^{11}$ to $10^{13}$ molecule $s^{-1}$ $cm^{-2}$. For both types of substrates, $F_L$ seems to be zero order in HCl for pulses exceeding $10^{15}$ molecules per pulse, that is, when the HCl/ice interface is in the liquid state.[12] We believe this "saturation" of $F_L$ at large HCl doses displayed in Figure 4 to be an artifact caused by the limiting value of the evaporation rate occurring at doses for which the HCl/ice interface becomes liquidlike. In the region below $2 \times 10^{15}$ HCl molecules per pulse, the rate law for $F_L$ seems to be proportional to the number of HCl in an individual pulse and thus is first order in HCl, as indicated in the inset of Figure 4. For SC samples, $F_L$ may be smaller ($5 \times 10^{11}$ to $3 \times 10^{12}$ molecule $s^{-1}$ $cm^{-2}$) than that for B ($10^{12}$−$10^{13}$ molecule $s^{-1}$ $cm^{-2}$) in the HCl concentration range in which $F_L$ is first order in HCl, most probably because of the different structure of the interface discussed below. The values of $F_L$ measured at low doses such as $10^{14}$ molecules per pulse are getting close to the limit of the experimental measurement capability.

*$F_L$ for $D_2O$ on Bulk (B) and Single-Crystal Ice (SC) at 200 K.* Figure 5 displays $F_L$ as a function of the individual dose per pulse for the $D_2O/H_2O$ system on B and SC ice at 200 K. No dependence of $F_L$ on the dose can be observed for SC samples. The effect of the nature of the ice substrate is more apparent than in the case of HCl; $F_L$ is 2 orders of magnitude larger for B ($4 \times 10^{14}$ molecule $s^{-1}$ $cm^{-2}$) than for SC ($6 \times 10^{12}$ molecule $s^{-1}$ $cm^{-2}$). The data for both types of ice (B and SC) are consistent with a zero-order dependence of $F_L$ on the individual dose of $D_2O$ up to $2 \times 10^{15}$ molecules per pulse, contrary to HCl ($m = 1$ in Figure 4).

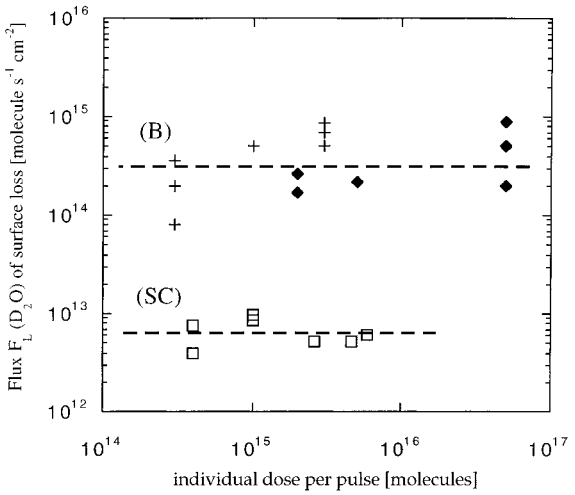


**Figure 5.** Flux $F_L$ of $D_2O$ surface-to-bulk loss at 200 K on bulk ice (B) (♦) and single-crystal ice (SC) (□), as a function of the individual dose per pulse. Crosses are measurements made on ice by cooling liquid water at a rate of −1 K/min.

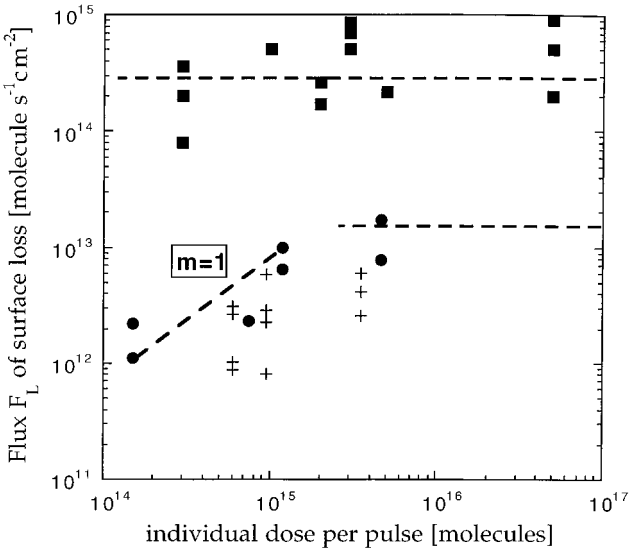


**Figure 6.** Comparison of flux $F_L$ of surface-to-bulk loss of $D_2O$ (■), HCl (●), and HBr (crosses) on bulk ice (B) samples at 200 K.

*$F_L$ for HBr and $D_2O$ on Bulk Ice (B) at 200 K.* Figure 6 displays the values of $F_L$ as a function of the individual dose for HBr and $D_2O$ on bulk ice (B) at 200 K. The HCl results are displayed for the sake of comparison. The $F_L$ values for $D_2O$ are 2 orders of magnitude larger than those obtained in the HX/ice system. On the basis of the existing data for the HBr/ice interaction, we simply state that the $F_L$ values are smaller than those for HCl/ice.

Figures 4, 5, and 6 clearly show that the flux of surface-to-bulk loss $F_L$ is a function of the identity of the gas-phase species as well as of the structure of the interface of the ice sample. For both HCl and $D_2O$, the value of $F_L$ is smaller on single-crystal compared to bulk ice. This may be due to the fact that the SC surface is more ordered than the B surface, the former having a lower surface defect density, cracks or grain boundaries, thus restricting pathways towards surface-to-bulk diffusion.

**Temperature Dependence of $F_L$ for HCl and $D_2O$ on Bulk Ice**. Figure 7 displays the temperature dependence of the flux of $F_L$ in the temperature range of 190−210 K for HCl and 170−

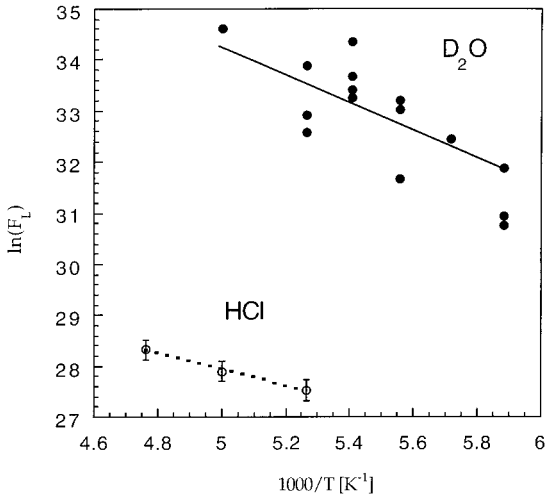


**Figure 7.** Arrhenius representation of the flux $F_L$ of surface-to-bulk loss of $D_2O$ (●) and HCl (○). For $D_2O$ and HCl, activation energy values of $E_A = 5.3 \pm 0.7$ and $3.0 \pm 0.5$ kcal/mol were found from least-squares fitting (solid and dashed lines, respectively).

200 K for $D_2O$. The Arrhenius representation leads to a positive activation energy $E_A$ of $F_L$ for both HCl and $D_2O$. $E_A$ for HCl and $D_2O$ is equal to $3.0 \pm 0.5$ and $5.3 \pm 0.7$ kcal/mol, respectively. Such values are consistent with those of bulk diffusion, as observed for instance on small ice particles by Mizuno et al.[14] Livingston et al.,[15] who studied the diffusion of HDO into single-crystal $H_2{}^{16}O$ ice multilayers using laser-induced thermal desorption, have reported an activation energy for surface diffusion ranging from 3.7 to 6.4 kcal/mol. This latter value may not necessarily be compared to our value for bulk $D_2O$ ice.

### Dope and Probe Experiments: Probing the HCl Concentration at the Ice Interfacial Region Using the Reaction $ClONO_2 + HCl \rightarrow Cl_2 + HNO_3$

The goal of this series of experiments is to validate the results obtained in RPEs by probing the HCl concentration at the interface, a region of finite thickness close to the surface of the ice sample. We dope an ice surface with HCl gas and probe for near-surface HCl that is "visible" from the gas phase using the fast titration reaction $ClONO_2 + HCl(s) \rightarrow Cl_2 + HNO_3$. By doping a pure ice surface with a known amount of HCl and varying the time delay for subsequent reactive $ClONO_2$ uptake monitored by $Cl_2$, we were able to measure the change of the HCl interfacial concentration with time using a mass balance argument; the yield of $Cl_2$ formed in reaction R-1 and its change with time since the start of the doping is an indirect probe of the change of the near-surface concentration of HCl with time. Therefore, a direct comparison with the flux $F_L$ of the surface-to-bulk loss process as observed in RPEs may be undertaken.

Studies performed on the interaction of alkali halide salts with $ClONO_2$ have shown that it displayed a pronounced "sticky" behavior and that the value of its uptake coefficient was independent of the structural characteristics of the substrate such as the Brunauer−Emmett−Teller (BET) surface area of the salt substrate.[16] This suggests that $ClONO_2$ primarily interacts with the external surface regardless of its microstructural details such as the presence of pores.[5] We therefore assume that $ClONO_2$ preferentially probes the gas−solid interface of ice whatever its nature may be without delving into the microstructural details of ice such as pores, cracks, grain boundaries, or imperfections. Thus $ClONO_2$ is thought to be the probe molecule of choice for exploring the surface and near-surface concentrations of HCl.

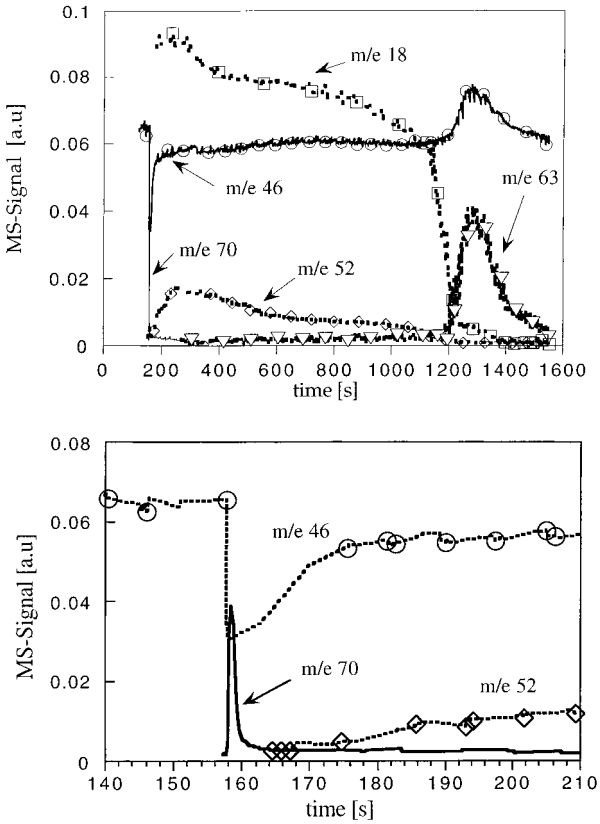


**Figure 8.** (top) HCl probing experiments on condensed ice (C) at 200 K using $ClONO_2$ in reaction R-1. $Cl_2$ is monitored at *m/e* 70 (thin solid line), $ClONO_2$ at *m/e* 46 (bold solid line, ○), HOCl at *m/e* 52 (◇), $HNO_3$ at *m/e* 63 (▽), $H_2O$ at *m/e* 18 (□). (bottom) Focus on the beginning of the titration reaction on a short time scale. The symbols are the same as above with $Cl_2$ displayed using the bold solid line.

Many studies of the heterogeneous interaction of $ClONO_2$ on ice doped with HCl have been performed to date.[17−19] Uptake coefficients were found to be dependent on the HCl concentration on the surface, with an upper limit of $\gamma = \sim 0.3$ in the temperature range of 180−200 K. Nitric acid, the condensed-phase product of reactions R-1 and R-2, is known to form thermodynamically stable hydrates in the present temperature and concentration regime, such as $HNO_3 \cdot 3H_2O$ (NAT) or $HNO_3 \cdot H_2O$ (NAM).[20−24] Recently, Zondlo et al.[3] suggested that the reaction of $ClONO_2$ on ice may lead to an amorphous $H_2O$/$HNO_3$ layer over the ice surface before crystallizing to a stable $HNO_3$ hydrate.

Figure 8 displays a typical experiment, performed at 200 K on a condensed ice sample (C). After the surface was doped at a HCl flow of $6 \times 10^{14}$ molecule $s^{-1}$ for 1 min leading to a HCl coverage of roughly two nominal monolayers, a continuous $ClONO_2$ flow of $10^{15}$ molecule $s^{-1}$ monitored at *m/e* 46 ($NO_2^+$) enters the reactor at $t = 158$ s and reacts with the HCl/ice sample according to reaction R-1. The MS signal at *m/e* 46 rapidly drops corresponding to an initial value of $\gamma_0 = 0.1$. At the same time, a prompt rise of molecular chlorine (*m/e* 70) is observed as shown in the bottom trace of Figure 8. For these continuous-flow experiments, molecular chlorine is the sole product detected at the beginning of the reaction. The $Cl_2$ signal decreases on a time scale of 5−10 s to a low and slowly decreasing level ultimately tending toward the $Cl_2$ impurity level in $ClONO_2$ on the time scale of a few minutes. HOCl gradually appears in the aftermath of the main $Cl_2$ production burst and slowly tends toward a steady-state value which is proportional to the rate of uptake of $ClONO_2$. These results are consistent with the ones

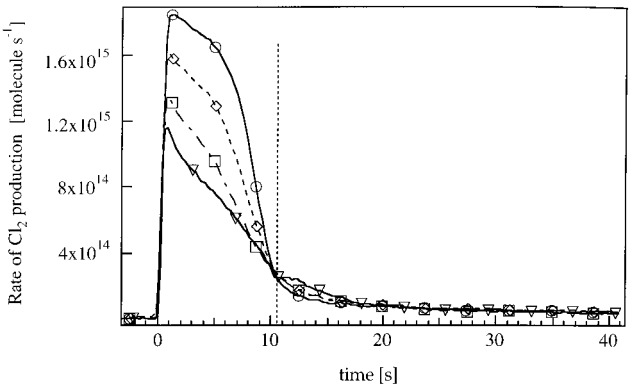


**Figure 9.** Main burst of $Cl_2$ production at 200 K for different time delays between doping and probing: 2 min (solid line, ○), 5 min (dashed line, ◇), 10 min (dashed line, □), and 20 min (solid line, ▽). The dividing line between interfacial HCl titration and bulk-to-interface back-diffusion has been set at the crossing point of the four traces.

presented in the literature.[25] During hydrolysis (R-2), the MS signal of $H_2O$ (*m*/*e* 18) decreases at $t = 5$ min to a lower partial pressure, accompanied by an increase in the surface coverage of $HNO_3$. Hanson[26] obtained the same result when he observed a phase transformation from an amorphous to a crystalline phase in flow tube experiments upon increasing the coverage of $HNO_3$ on ice. The MS signal at *m*/*e* 18 slightly decreases as long as the hydrolysis reaction continues in the range of $t = 10-20$ min. At the same time, a small amount of nitric acid (*m*/*e* 63) appears in the gas phase. At $t = 20$ min, the $H_2O$ and HOCl signals suddenly drop, indicating the end of the $H_2O$ supply for hydrolysis. The total $HNO_3$ previously stored in the condensed phase during reactions R-1 and R-2 is released into the gas phase. However, for the present purpose we focus on the main burst, that is, the large rate of $Cl_2$ appearance, followed by a lower rate of $Cl_2$ formation.

### Results of Dope and Probe Experiments

We studied the time dependence of the rapid chlorine production ("burst") as a function of the time delay between the end of the HCl−ice doping and the beginning of the probing using $ClONO_2$, whose flow was $\sim 10^{15}$ molecule $s^{-1}$ (Figure 8, bottom). Figure 9 shows raw MS signals of $Cl_2$ monitored at *m*/*e* 70 during the initial uptake of $ClONO_2$ for various time delays ranging from 2 to 20 min between HCl doping and $ClONO_2$ probing on bulk ice (B) at 190 K. The experiments were performed on the same ice sample after regeneration of the sample by thermal desorption of $HNO_3$ between each doping/probing series. Approximately $1.6 \times 10^{16}$ molecules of HCl corresponding to one formal monolayer were taken up before the start of $ClONO_2$ probing. The *fractional* yield $Y(Cl_2)$ of $Cl_2$ production is defined as $N(Cl_2)/N(HCl)$ where $N(Cl_2)$ and $N(HCl)$ are the integrals of the MS traces between $t = 0$ and 10.5 s of the $Cl_2$ production rate and the total number of HCl previously taken up, respectively. $Y(Cl_2)$ decreases as a function of increasing time delay between doping and probing as indicated in Table 2 and Figure 10. Moreover, the duration of the main burst of chlorine is more or less equal to 10 s at a given $F^i(ClONO_2)$ of $4 \times 10^{15}$ molecule $s^{-1}$ and seems to be independent of the time delay. On the other hand, the *total* chlorine yield, namely, the sum of the initial main burst and the subsequent yield corresponding to the low rate of production in the tail, indicates a 1:1 correspondence between reactant lost and product formed in all experiments, whatever the time delay. This latter fact shows nothing other than a closed mass balance for total $Cl_2$ produced.

**TABLE 2: Observed Fractional Yield $Y(Cl_2)$ of $Cl_2$ on Single-Crystal Ice (SC) and on Bulk Ice (B) at 190 and 200 K as a Function of the Time Delay between the End of the HCl Doping and the Start of Probing Using Reaction R-1[a]**

| ice sample | $T$ [K] | delay $t$ [min] | $N$(HCl) | $N(Cl_2)$ | $Y(Cl_2)$ [%] |
|---|---|---|---|---|---|
| SC | 190 | 2 | $1.5 \times 10^{16}$ | $1.47 \times 10^{16}$ | 98 |
| | 190 | 3 | $1.5 \times 10^{16}$ | $1.41 \times 10^{16}$ | 94 |
| | 190 | 5 | $1.5 \times 10^{16}$ | $1.44 \times 10^{16}$ | 96 |
| | 190 | 7 | $1.5 \times 10^{16}$ | $1.39 \times 10^{16}$ | 93 |
| B | 190 | 2 | $1.6 \times 10^{16}$ | $1.7 \times 10^{16}$ | 100 |
| | 190 | 4 | $1.6 \times 10^{16}$ | $1.3 \times 10^{16}$ | 88 |
| | 190 | 5 | $1.6 \times 10^{16}$ | $1.35 \times 10^{16}$ | 90 |
| | 190 | 6 | $1.6 \times 10^{16}$ | $1.2 \times 10^{16}$ | 76 |
| | 190 | 10 | $1.6 \times 10^{16}$ | $1.12 \times 10^{16}$ | 70 |
| B | 200 | 1 | $1.1 \times 10^{16}$ | $1.0 \times 10^{16}$ | 90 |
| | 200 | 5 | $1.1 \times 10^{16}$ | $0.66 \times 10^{16}$ | 60 |
| | 200 | 7 | $1.1 \times 10^{16}$ | $0.58 \times 10^{16}$ | 53 |
| | 200 | 10 | $1.1 \times 10^{16}$ | $0.44 \times 10^{16}$ | 40 |

[a] $N$(HCl) is the number of HCl taken up on the ice surface; $N(Cl_2)$ is the number of $Cl_2$ product molecules integrated from 0 to 10 s (see Figure 9).

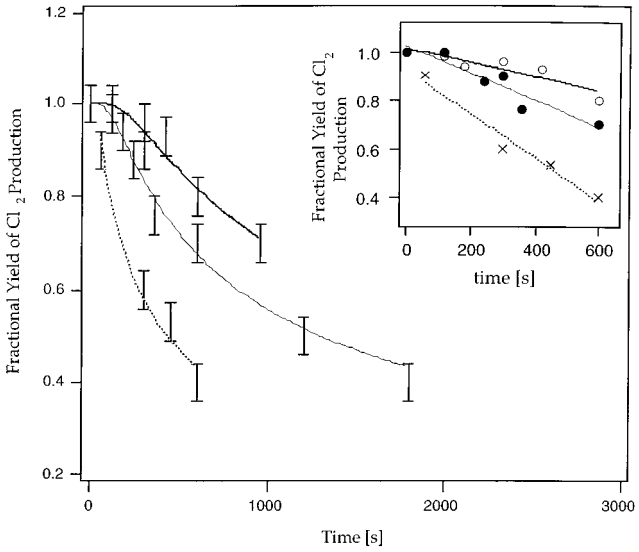


**Figure 10.** Fractional yield of $Cl_2$, $Y(Cl_2)$, as a function of the time delay between HCl doping and $ClONO_2$ probing on SC (○) and B (●) at 190 K and B (×) at 200 K. The lines are fits using Fick's second law (see text). The inset on the upper right-hand corner presents $Y(Cl_2)$ on the time scale from 0 to 600 s and shows $Y(Cl_2)$ to be linearly dependent on the time delay to a good approximation. The three lines are least-squares fits.

We interpret the initial rapid $Cl_2$ production as resulting from the reaction of $ClONO_2$ with HCl present in the interface region and available for titration without delay. The shape as well as the duration of the initial chlorine production, compared to the subsequent low rate of production, suggest that the interfacial region is a well-defined HCl reservoir, characterized by a thickness $h$ and a HCl mole fraction $X_{HCl}$. The longer the time delay between doping and probing, the larger the number of HCl molecules which have disappeared from the interface into the bulk by surface-to-bulk loss. When the interface becomes depleted in HCl at $t = 10$ s, the low rate of $Cl_2$ production after the main burst is interpreted as the rate-limiting process of HCl back-diffusion from the bulk to the interface region where it is available for reaction with $ClONO_2$ in reaction R-1. Such experiments reveal the time-dependent HCl partitioning in the ice sample and its reactivity toward $ClONO_2$. Measurements were made on SC and B ice at 190 K and on B ice at 200 K to

**TABLE 3: Flux of Surface-to-Bulk Loss $F_L$ Obtained in Dope and Probe Experiments of HCl**

| ice sample | $T$ [K] | $F_L$[molecule $s^{-1}$ $cm^{-2}$] |
|---|---|---|
| SC | 190 | $(2 \pm 1) \times 10^{11}$ |
| B | 190 | $(7 \pm 3) \times 10^{11}$ |
| B | 200 | $(9 \pm 3) \times 10^{11}$ |

evaluate the time dependence of the HCl concentration at the interface of the ice substrate.

The present data allow us to obtain a value of the flux of surface-to-bulk loss and consequently validate the previous RPEs. In the discussion below, we present an evaluation of the thickness $h$, derived from similar dope and probe experiments. We thus propose a description according to the laws of Fickian diffusion leading to the determination of the diffusion coefficient $D_{HCl}$ in ice.

**Linear Regime: Measurement of $F_L$ and Comparison with RPEs.** Figure 10 displays the fractional yield $Y(Cl_2)(t)$, defined as $N(Cl_2)(t)/N(HCl)$ of $Cl_2$ as a function of the time delay $t$ between HCl doping of the interface and probing by $ClONO_2$ in titration experiments. The dependence of $Y(Cl_2)$ on the time delay $t$ is the manifestation of the decrease of the HCl concentration in the interface region owing to diffusion into the bulk. We focus below on the time dependence of $Y(Cl_2)$ on the time scale of 0−600 s displayed in the upper right-hand corner of Figure 10, which can be fitted to a *linear* function of the time delay $t$. The linear fit is equivalent to assuming that $F_L$ is independent of time over the range of 0−600 s. The number of $Cl_2$ generated in the burst displayed in Figure 9 following reaction R-1, that is, $N(Cl_2)$, may be described as a function of the time delay $t$ between HCl doping and $ClONO_2$ probing according to

$$N(Cl_2)(t) = N(HCl) - F_L A_s t \qquad (1)$$

where $A_s$ is the geometric surface of the ice sample (Table 1). It has to be kept in mind that $N(Cl_2)(t)$ results from the integration over the main burst of $Cl_2$ formation whose duration is approximately 10 s and $t$ is the elapsed time between HCl doping and $ClONO_2$ probing ranging from 2 to 10 min. $N(Cl_2)(t)$ may thus be considered a direct measure of the time-dependent interfacial HCl concentration within the interface thickness $h$. The flux of surface-to-bulk loss ($F_L$) is given by the slope of the least-squares fit displayed in the inset of Figure 10 (data in Table 3). The linear time dependence of $Y(Cl_2)$ in the time interval 0−600 s obtains a value of $F_L$ for HCl according to eq 1 which are in remarkable agreement with the values obtained from RPEs performed using individual doses of less than $10^{15}$ molecules per pulse (Figure 4) and are thus providing a consistent picture of the HCl/ice interfacial region based on two very different kinds of experiments.

## Discussion

On one hand, dope and probe experiments confirm the existence of a loss process of HCl from the ice surface into the bulk which has already been revealed in RPEs. On the other hand, they suggest, as will be discussed below, that the interfacial region is a well-defined HCl reservoir characterized by a thickness $h$ and a HCl mole fraction $X_{HCl}$. In the following, we discuss how $h$ and $X_{HCl}$ may be experimentally derived in dope and probe experiments. Finally, both $h$ and $X_{HCl}$ are used to fit the time-dependent data displayed in Figure 10 according to the laws of diffusion, allowing the assessment of the diffusion coefficient $D_{HCl}$ for B, C, and SC ice substrates.

**TABLE 4: Calculated ((a) and (b)) and Experimental (expt) HCl Mole Fraction $X_{HCl}$ at 190 and 200 K on a Sample Co-condensed from $H_2O$ and HCl Vapor Using a Flow Reactor with an Orifice Diameter of 4 mm[a]**

| $T$ [K] | $P_{HCl}$ [Torr] | $P_{H_2O}$ [Torr] | $X_{HCl}$(a) | $X_{HCl}$(b) | $X_{HCl}$(expt) |
|---|---|---|---|---|---|
| 190 | $1.1 \times 10^{-5}$ | $6.3 \times 10^{-3}$ | $2.9 \times 10^{-4}$ | $7.4 \times 10^{-4}$ | $1.24 \times 10^{-3}$ |
| 200 | $3.6 \times 10^{-6}$ | $4.4 \times 10^{-3}$ | $4.9 \times 10^{-4}$ | $3.5 \times 10^{-4}$ | $6.7 \times 10^{-4}$ |

[a] Values for $X_{HCl}$(a) and $X_{HCl}$(b) are calculated according to eqs 2 and 3, respectively, with $\alpha(H_2O) = 0.5$ and $\alpha(HCl) = 0.3$.

**Determination of the HCl Mole Fraction $X_{HCl}$ in the Interface Region.** Numerous studies report values of the solubility of HCl in ice[27−29] which are in the range of $X_{HCl} = 10^{-5}-10^{-4}$ at 200 K for a HCl partial pressure of $\sim 10^{-5}$ Pa. More recently, Thibert and Dominé[30] investigated the thermodynamics and kinetics of solid solutions of HCl in ice in the temperature range of −35 to −8 °C. They recommended the following relationship for the calculation of HCl solubility with $P$ in Pa:

$$X_{HCl} = (6.13 \times 10^{-10})\, e^{(2806.5/T)}\, (P_{HCl})^{1.2/73} \qquad (2)$$

These authors also proposed eq 3 for cases in which the incorporation of HCl is controlled by the kinetics of condensation:

$$X_{HCl} = \frac{P_{HCl}}{P_{H_2O}} \frac{\alpha_{HCl}}{\alpha_{H_2O}} \left[\frac{M_{H_2O}}{M_{HCl}}\right]^{1/2} \qquad (3)$$

The parameters $\alpha_{HCl}$ and $\alpha_{H_2O}$ are the mass accommodation coefficients for HCl and $H_2O$, respectively, at a given temperature. Table 4 displays calculations of $X_{HCl}$ according to eqs 2 and 3.

To obtain a value of $X_{HCl}$ for our experimental conditions, we performed ancillary HCl/$H_2O$ co-deposition experiments. We concurrently condensed $H_2O$ and HCl at $T = 190$ K onto the cold support at typical flow rates of $10^{17}$ and $10^{14}$ molecule $s^{-1}$, respectively. The duration of the co-deposition was ∼5 min, leading to a deposit thickness of at least 1 $\mu$m. The composition of such a sample is assumed to be homogeneous and is given by the relative amount of each compound deposited on the cold substrate which could be measured experimentally. Table 4 shows the HCl mole fraction measured from co-condensation experiments at 190 and 200 K and the comparison with calculations according to eqs 2 and 3. Calculated and experimental values for $X_{HCl}$ are in reasonably good agreement. In the remainder of this discussion, we use the experimental value $X_{HCl}$ (expt) of Table 4 for the fitting of the dope and probe data. For B and SC ice samples, the experimental determination of $X_{HCl}$ was not possible by said mass balance argument. In this case, we used the $X_{HCl}$ values obtained above on the C ice sample for comparable HCl partial pressures.

Figure 11 displays a dope and probe experiment on a co-condensed HCl/$H_2O$ (C*) sample at 190 K at a $ClONO_2$ flow rate of $6 \times 10^{15}$ molecule $s^{-1}$. The main burst of $Cl_2$ production lasts for ∼20 s and is followed by a $Cl_2$ steady-state flow rate of 300 s, which ultimately decreases toward the level of the small $Cl_2$ impurity in $ClONO_2$ when the HCl/ice sample is vanishing upon pumping according to reactions R-1 and R-2. We note the high rate of $Cl_2$ production in the aftermath of the $Cl_2$ burst in contrast to the much lower rate of $Cl_2$ production observed on C and B samples (Figures 8 and 9), in which the bulk was essentially free of HCl. Figure 11 surprisingly reveals that the HCl/$H_2O$ co-condensed sample is not homogeneous

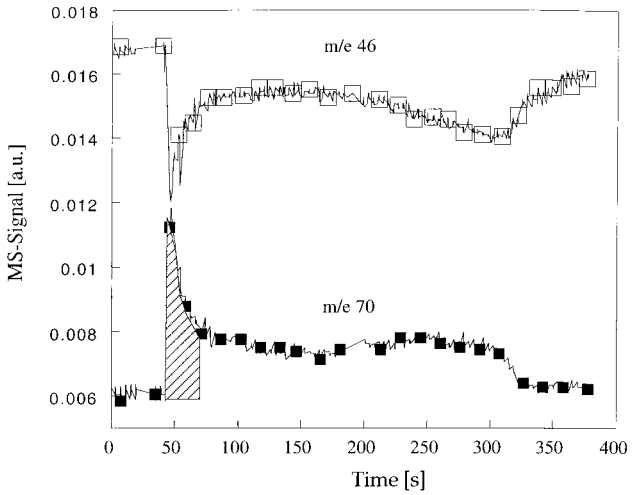


**Figure 11.** Exhaustive $ClONO_2$ uptake experiment on a $HCl/H_2O$ co-condensed sample (C*) at 190 K at flow rates of $10^{17}$ and $10^{14}$ molecule $s^{-1}$ of $H_2O$ and HCl, respectively. The flow of $ClONO_2$ was $6 \times 10^{15}$ molecule $s^{-1}$ (□). $Cl_2$ production (■) and uptake of $ClONO_2$ stop at $t = 340$ s owing to vanishing ice supply.

throughout. The rate of $Cl_2$ formation is higher at the beginning of the HCl titration by $ClONO_2$, corresponding to the hatched area in Figure 11. This indicates the presence of an interfacial region where none is expected owing to the seemingly homogeneous sample generated from the co-deposition of HCl and $H_2O$ whose uptake coefficients are very similar under the chosen experimental conditions. This result suggests that the ice matrix controls at least in part the properties of the HCl/ice interface. Hydrolysis of $ClONO_2$ becomes competitive when the HCl concentration in the interfacial region is sufficiently depleted. Rate-limiting back-diffusion of HCl from the bulk toward the interface sets in after the main burst of 20 s duration.

**Thickness *h* of the Interface Region.** The thickness of the interface region was estimated in three ways as described by (a), (b), and (c) below.

(a) The number of HCl molecules $N(HCl)$ taken up into the interfacial region leads to a $HCl/H_2O$ mixture of mole fraction $X_{HCl} = N(HCl)/(N(HCl) + N(H_2O)) \cong N(HCl)/N(H_2O)$ in a region of thickness $h$. The number of nominal monolayers of individual thickness $d$ composing the ice matrix of the interfacial region may be expressed as $N(H_2O)$ divided by the $H_2O$ surface site density of $1.07 \times 10^{15}$ $cm^{-2}$. [31] Thus

$$h = \left[\frac{N(HCl)/X_{HCl}}{1.6 \times 10^{16}}\right] d \qquad (4)$$

where $1.6 \times 10^{16}$ is the total number of surface molecules of $H_2O$ for our surface area of 15 $cm^2$ and $d$ is the thickness of one nominal layer of water ice and is estimated to be equal to 0.4 nm.[44] Table 5 displays calculated values for $h$ according to eq 4 labeled as $h$(a) using experimentally determined values of $N(HCl)$ from dope and probe experiments and $X_{HCl}$ measured in co-deposition experiments as described above; $X_{HCl}$ was assumed to be independent of the type of ice.

(b) We also experimentally determined the thickness of the interface region using kinetic measurements by means of converting the reaction time into a thickness; Figure 12 summarizes the processes occurring in dope and probe experiments. In the first step, $ClONO_2$ reacts with HCl located in the interfacial region in a rapid process or main burst without the incidence of a precursor, which is characterized by a high uptake coefficient of ~0.1. In all experiments performed to date, the duration $t_1$ of this stage was a few seconds. After the initial $Cl_2$ burst has subsided, the interfacial ice matrix is devoid of HCl and $ClONO_2$ starts to be hydrolyzed by $H_2O$ in the presence of $HNO_3$ generated in reaction R-1. Concomitantly, back-diffusion of HCl occurs from the bulk toward the interface which is revealed by the slow release of $Cl_2$ in the tail of the dope and probe experiments (Figure 9). The duration $t_2$ of the slow hydrolysis depends on the total thickness $l$ of the ice sample as well as on the used $ClONO_2$ flow and is typically 15−20 min (Figure 8).

The hydrolysis, reaction R-2, starts when the interfacial ice matrix is low in HCl, that is, at $t \geq t_1$. Both the pseudo-first-order rate constant $k_1$ for titration at excess $ClONO_2$ and the initial pseudo-first-order rate constant $k_2$ for hydrolysis have been measured for every dope and probe experiment, and the relationship $k_2 \approx {}^1/_6 k_1$ has been established. The interfacial ice matrix composed of $(N(HCl)/X_{HCl})$ $H_2O$ molecules will be consumed by hydrolysis within $t_1$ at approximately the following rate:

$$-\frac{dN(H_2O)}{dt} = \frac{N(HCl)/X_{HCl}}{t_1}\left(\frac{k_2}{k_1}\right) \qquad (5)$$

Equation 5 is an approximation, because $k_1$ is assumed to be constant over the duration 0 to $t_1$. Figure 8 reveals that this approximation should hold to a factor of >2 for both $k_1$ and $k_2$, considering the signal level for $ClONO_2$ at $m/e$ 46 between 158 and 162 s, which corresponds to the end of the $Cl_2$ burst. The rate of hydrolysis may be written using the kinetic rate law according to eq 6, considering the rate of hydrolysis and the rate of evaporation $R_{evap}$ of $H_2O$ upon pumping through the escape orifice without balancing $H_2O$ flow:

$$-\frac{dN(H_2O)}{dt} = k_2[ClONO_2]V + R_{evap} \qquad (6)$$

By setting eq 6 equal to eq 5 and using eq 4, the thickness $h$ may be finally expressed as

$$h = (k_2[ClONO_2]V + R_{evap})\left(\frac{k_1}{k_2}\right) t_1 \frac{d}{1.6 \times 10^{16}} \qquad (7)$$

The calculated values for $h$ according to eq 7, labeled as $h$(b), are shown in Table 5. The values of $k_1$ and $k_2$ were determined to be 3.5 and 0.6 $s^{-1}$, respectively. We used the values found by Chaix et al.[11] for the rate of evaporation of $H_2O$ of $1.6 \times 10^{16}$ molecule $s^{-1}$ $cm^{-2}$ at 190 K and $3.5 \times 10^{16}$ molecule $s^{-1}$ $cm^{-2}$ at 200 K for condensed ice samples (C). For bulk ice (B) samples, $R_{evap}$ was found to be $3.5 \times 10^{16}$ molecule $s^{-1}$ $cm^{-2}$ at 190 K and $1 \times 10^{17}$ molecule $s^{-1}$ $cm^{-2}$ at 200 K. For single-crystal ice (SC) at 190 K, $R_{evap} = 8 \times 10^{15}$ molecule $s^{-1}$ $cm^{-2}$ was used. For co-condensed $HCl/H_2O$ samples (C*), the number $N(HCl)$ of HCl molecules located in the interfacial region at the interface has been indirectly determined from the mass balance assuming a 1:1 correspondence between main burst $Cl_2$ production and HCl lost (Figure 11).

(c) We have observed a good correlation between the duration $t_2$ of hydrolysis and the number of $H_2O$ molecules constituting the thin film ice sample on condensed (C) ice, under conditions of constant $ClONO_2$ flow. The duration $t_2$ is equal to the total thickness $l$ of the condensed sample divided by the rate of hydrolysis, expressed in monolayers per unit time, whereas the duration $(k_1/k_2)t_1$ is equal to the interfacial thickness $h$ divided by the rate of hydrolysis under the same pumping conditions.

**TABLE 5: Calculated Values of the Interfacial Thickness *h* Using (a) Eq 4, (b) Eq 7, and (c) Eq 8[a]**

| ice | $T$ [K] | $N$(HCl) [molecules] | $N$($H_2O$) [molecules] | $F^i$($ClONO_2$) [molecule $s^{-1}$] | $t_1$ [s] | $t_2$ [s] | $h$(a) [nm] | $h$(b) [nm] | $h$(c) [nm] | $l$ [$\mu$m] |
|---|---|---|---|---|---|---|---|---|---|---|
| C* | 190 | $4 \times 10^{15}$ | $9.4 \times 10^{19}$ | $6 \times 10^{15}$ | 10 | 300 | 82 | 350 | 447 | 2.3 |
| C* | 200 | $6.9 \times 10^{15}$ | $3.8 \times 10^{19}$ | $3.75 \times 10^{15}$ | 10 | | 258 | 766 | | 0.9 |
| C | 190 | $2.5 \times 10^{16}$ | $1.5 \times 10^{20}$ | $3.8 \times 10^{15}$ | 7 | 660 | 500 | 258 | 238 | 3.8 |
| C | 190 | $1.3 \times 10^{16}$ | $2.8 \times 10^{20}$ | $4.4 \times 10^{15}$ | 6 | 220 | 260 | 222 | 314 | 7.0 |
| C | 190 | $1.9 \times 10^{16}$ | $3.3 \times 10^{20}$ | $4.8 \times 10^{15}$ | 5 | 1100 | 380 | 186 | 224 | 8.2 |
| C | 190 | $1.3 \times 10^{16}$ | $5.5 \times 10^{19}$ | $5.2 \times 10^{15}$ | 7 | 240 | 260 | 260 | 240 | 1.3 |
| C | 190 | $1.3 \times 10^{16}$ | $1 \times 10^{20}$ | $5.2 \times 10^{15}$ | 7 | 414 | 260 | 260 | 252 | 2.5 |
| C | 190 | $1.2 \times 10^{16}$ | $1 \times 6^{20}$ | $6.5 \times 10^{15}$ | 3 | 1400 | 240 | 112 | 50 | 4.1 |
| B | 190 | $1.6 \times 10^{16}$ | | $4.8 \times 10^{15}$ | 11 | | 320 | 878 | | bulk |
| B | 200 | $9 \times 10^{15}$ | | $3.9 \times 10^{15}$ | 5 | | 335 | 1128 | | bulk |
| SC | 190 | $1.4 \times 10^{16}$ | | $4.8 \times 10^{15}$ | 5 | | 280 | 96 | | SC |

[a] Ice samples are HCl/$H_2O$ co-condensed (C*), condensed (C), bulk (B), and single-crystal (SC). The calculation for $h$(a) according to eq 4 was made using the experimental value of $X_{HCl}$ displayed in Table 4.

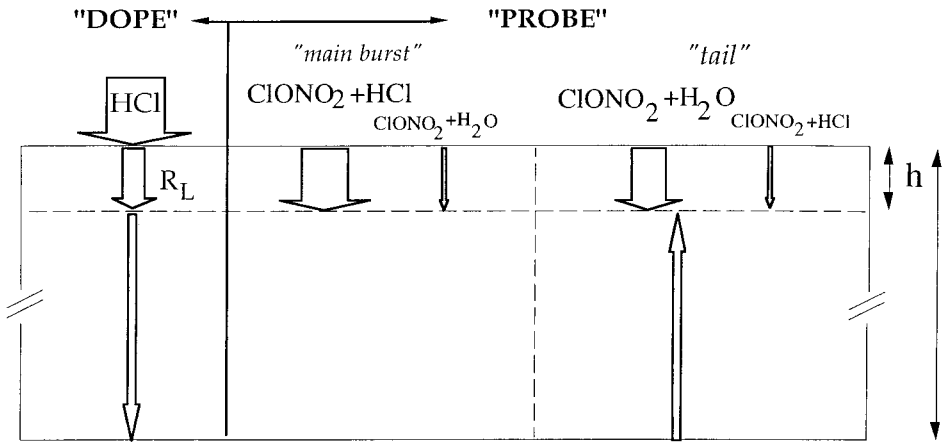


**Figure 12.** Schematic cross-sectional view of a condensed ice sample. $h$ and $l$ are the thicknesses of the interfacial region and the sample, respectively. The widths of the arrows represent the rates of reaction or diffusion.

Assuming that the rate of hydrolysis is equal for $H_2O$ located in the interfacial region and for $H_2O$ making up the bulk of thickness $l$, we may write

$$\frac{h}{l} = \frac{t_1(k_1/k_2)}{t_2} \quad \text{or} \quad h = l\left(\frac{t_1}{t_2}\right)\left(\frac{k_1}{k_2}\right) \tag{8}$$

The calculated values for $h$ according to eq 8, $h$(c), are shown in Table 5. We thus have used three different methods to assess the thickness of the interface $h$ using eqs 4, 7, and 8. On C ice samples, $h$ was calculated using all three methods, whereas on B and SC samples method (c) using eq 8 has not been used because of the large value of $l$.

Table 5 summarizes the calculated values for the interfacial thickness for C*, C, B, and SC ice samples. The values for $h$ calculated according to eq 4 using the experimental value for $X_{HCl}$ and eqs 7 and 8 are in reasonable agreement. For C samples, eq 4 obtains $h$ values larger by up to a factor of 2 compared to those based on kinetic arguments (eq 7), which may be related in part to the factor of 2 uncertainty in the reaction rates R-1 and R-2 discussed above. One reason may be that $X_{HCl}$ at the interface is underestimated by assuming it to be representative for the bulk. Huber et al.[32] reported measurements of relatively high HCl concentrations (0.2 wt %) near the ice surface for samples that had been in contact with aqueous solutions. In summary, the use of eq 7 reveals a substrate dependence of $h$. For single-crystal ice at 190 K, $h$ is ~100 nm; $h$ is ~200 nm on condensed ice and ~1 $\mu$m for bulk ice. Owing to the narrow temperature range, no dependence of $h$ on temperature could be observed. Perhaps surprising is the relatively large value of $h$ on all three studied ice substrates as far as the HCl/ice interfacial region is concerned. This result should be kept in mind when studying interfaces using spectroscopic investigations of ultrathin samples at similar temperatures.

**Diffusion Coefficient *D* for HCl in Ice.** *Fick's First Law.* We interpret our data by identifying the kinetics of the gas/condensed phase loss process of HCl given by $F_L$ with the interface/bulk process described by the laws of diffusion. Fick's first law, eq 9, describes a stationary process and was used to

$$J = -D_{HCl}\frac{\partial C(x,t)}{\partial x} \tag{9}$$

interpret the data obtained in RPEs by setting $J$ equal to $F_L$. In eq 9, $J$ is the net flux of HCl through the plane given by the ice sample. $D_{HCl}$ is the diffusion coefficient of HCl, and $\partial C(x,t)/\partial t$ is the concentration gradient across the ice sample. We limit the following discussion to only one-dimensional transport. The measurement of the spatial distribution of HCl in the interface region of thickness $h$ is not possible using the present experiments. As an approximation, the gradient of the concentration in eq 9 may be expressed by the known concentration of HCl taken up into the volume $V_{IF}$ of the interfacial region divided by its thickness $h$, thereby neglecting the HCl concentration built up in the bulk by the slow diffusion process during prior HCl doping:

$$\frac{\partial C(x,t)}{\partial x} = \frac{C(0,t) - C(h,t)}{h} \approx \frac{N(\text{HCl})}{V_{IF}h} \tag{9a}$$

**TABLE 6: Diffusion Coefficient $D_{HCl}$ as a Function of the Type of Ice, Calculated According to Fick's First Law (Eq 11) and Fick's Second Law (Eq 12) at $T = 190$ K[a]**

| | | | | $D_{HCl}$ [cm$^2$ s$^{-1}$] | |
|---|---|---|---|---|---|
| ice | $h$ [nm] | $F_L$ [molecule s$^{-1}$ cm$^{-2}$] | $X_{HCl}$ | Fick's first law | Fick's second law |
| SC | $100 \pm 10$ | $(2 \pm 1) \times 10^{11}$ | $(1.0 \pm 0.3) \times 10^{-3}$ | $(4.0 \pm 1.0) \times 10^{-14}$ | $(1.2 \pm 0.5) \times 10^{-14}$ |
| C | $200 \pm 50$ | $(7 \pm 3) \times 10^{11}$ | $(1.0 \pm 0.3) \times 10^{-3}$ | $(5.6 \pm 1.0) \times 10^{-13}$ | |
| B | $1000 \pm 200$ | $(7 \pm 3) \times 10^{11}$ | $(1.0 \pm 0.3) \times 10^{-3}$ | $(2.8 \pm 1.0) \times 10^{-12}$ | $(2.1 \pm 1.0) \times 10^{-12}$ |

[a] The value of $h$ is a mean value for a thickness $h$ calculated according to eq 7 (see values of $h$ (b) in Table 5).

Thus, the flux of surface-to-bulk loss $F_L$ is proportional to the steady-state concentration $N(HCl)/V_{IF}$ of HCl present in the interfacial region during continuous HCl flow or sufficiently fast repetitive injection like that in RPEs. Equation 10 is the defining equation for $D_{HCl}$ under the assumption of a linear HCl concentration gradient across the interfacial region:

$$D_{HCl} = F_L \frac{h}{N(HCl)} V_{IF} = F_L \frac{A_s h^2}{N(HCl)} \qquad (10)$$

Using the observed values of $N(HCl)$ and eqs 4 and 10, we obtain

$$D_{HCl} = F_L \left(\frac{h}{X_{HCl}}\right) (4 \times 10^{-23}) \qquad (11)$$

with $D_{HCl}$ expressed in cm$^2$ s$^{-1}$, $F_L$ in molecule cm$^{-2}$ s$^{-1}$, and $h$ in cm.

Equation 11 establishes the relationship between the measured flux of surface-to-bulk loss $F_L$ and the diffusion coefficient $D_{HCl}$ in ice, assuming a constant average HCl mole fraction in the interfacial region such as is the case in RPEs at a sufficiently rapid injection frequency.

Table 6 summarizes the values for the diffusion coefficient of HCl in ice, calculated according to eq 11, using the value of $h$(b) (Table 5) and $X_{HCl}$ measured from co-deposition experiments of "synthetic" HCl/$H_2O$ interfaces. Because of the large uncertainties, these values have to be considered as upper limits. The nature of the substrate seems to have a strong influence on $D_{HCl}$, with a difference of 2 orders of magnitude between values for SC and B. The surface-to-bulk processes seem to be well described by Fick's first law which assumes a constant HCl concentration in the gas phase, such as is approximately the case in RPEs and in dope and probe experiments on the time scale from 0 to 600 s.

*Fick's Second Law.* In dope and probe experiments, the gas-phase HCl concentration over the ice surface is vanishing during $ClONO_2$ probing. We have seen above that Fick's first law satisfactorily described the surface-to-bulk diffusion on the time scale over which $F_L$ could be considered as constant (eq 1). However, the time dependence of $Y(Cl_2)$ swerves out of a linear approximation at delays larger than 600 s (see Figure 10). The fact that the HCl reservoir atop the surface is vanishing affects the interfacial HCl concentration at long time delays in a way outlined by Fick's second law, which describes bulk diffusion for cases in which the interfacial concentration does not remain constant over time. The solution of Fick's second law leads to eq 12 with appropriate boundary conditions:[33]

$$C(x,t) = \frac{C_0}{2}\left[\mathrm{erf}\left(\frac{x+h}{2\sqrt{Dt}}\right) - \mathrm{erf}\left(\frac{x-h}{2\sqrt{Dt}}\right)\right] \qquad (12)$$

The initial conditions stipulate that the HCl concentration at $t = 0$ is confined to the interfacial region of thickness $h$:

$$C(x,0) = C_0 \qquad h \geq x \geq 0$$
$$C(x,0) = 0 \qquad x > h \qquad (12a)$$

Equation 12 describes the HCl concentration in the condensed phase for cases in which the surface concentration $C_0(t) = N(HCl)(t)/V_{IF}$ does not remain constant over time, as in the case of $ClONO_2$ probing experiments. The data we obtained for $Y(Cl_2)$ as a function of the time delay between doping and probing (Figure 10) can be fitted by eq 12 if we interpret the time-dependent value of $Y(Cl_2)$ as a probe for the interfacial concentration of HCl, expressed as $C(0,t)$ assumed to be constant over the interface thickness $h$. By setting the values of $h$(b) found for SC and B samples from Table 5, we obtain the following values for $D$: $2.1 \times 10^{-12}$ and $6.3 \times 10^{-12}$ cm$^2$ s$^{-1}$ for B at 190 and 200 K, respectively. For SC, we obtain $D = 1.2 \times 10^{-14}$ cm$^2$ s$^{-1}$ at 190 K, a value lower than that for B by 2 orders of magnitude. These values are displayed in Table 6 for comparison with the ones calculated using eq 11. They agree very well with our previous estimation based on the solution of Fick's first law and the analysis of RPEs.

*Comparison with the Literature.* Diffusion of HCl in ice has been studied in an atmospheric context by a wide variety of methods. Unfortunately, a very wide range of values has been obtained, largely owing to the wide range of water and HCl partial pressures used. Figure 13 shows a synopsis of selected values of $D_{HCl}$ in ice. In early work, Molina et al.[27] obtained a value for $D_{HCl}$ at 185 K of $\sim 10^{-9}$ m$^2$ s$^{-1}$. It is possible that the formation of a liquid layer at the ice surface resulting from the use of high HCl partial pressures may have affected this result. More recent experimental studies yield values between $10^{-16}$ and $10^{-14}$ m$^2$ s$^{-1}$ at this temperature, with one study resulting in $D_{HCl} < 10^{-13}$ cm$^2$ s$^{-1}$ at $-20$ °C.[34] Thibert and Dominé[30] found $D_{HCl}$ to be approximately $5 \times 10^{-12}$ cm$^2$ s$^{-1}$ on $I_h$ ice in the temperature range of $-35$ to $-8$ °C without an apparent temperature dependence. The latter results have been obtained by fitting diffusion profiles to spatially resolved concentration measurements (depth profiles). Horn and Sully[35] recently found a value of $D_{HCl} = 1.5 \times 10^{-15}$ m$^2$ s$^{-1}$ using ATR-IR spectroscopy on an ice film of thickness of $1-2$ $\mu$m.

Using eq 11, we assume that $D_{HCl}$ is proportional to $F_L$ on the time scale of our experiments. We thus estimate that the diffusion coefficient $D_{H_2O}$ for $H_2O$ is 2 orders of magnitude larger than $D_{HCl}$ at 200 K if we take our value for B ice (Figure 5) and a similar value of $h$, which comes very close to the value of the self-diffusion coefficient of $H_2O$ in macroscopic polycrystalline ice ($10^{-10}$ cm$^2$ s$^{-1}$ at 200 K[36]). The bulk diffusion of $H_2O$ in crystalline ice has been explored previously by many researchers.[37-43] Microtome and scintillation tracer techniques were used to measure the self-diffusion coefficients of $H_2{}^{18}O$, $D_2O$, and $T_2O$ in the temperature range of 238−273 K. The measured $H_2O$ diffusion coefficients were very similar for all the isotopic probe molecules with a typical value of $D \approx 2 \times 10^{-12}$ cm$^2$ s$^{-1}$ at $T = 263$ K.[44] Activation energies for $H_2O$ self-diffusion have ranged from $E_A = 12.4$ to 15.7 kcal/mol. In addition to the isotopic tracer experiments, in situ X-ray

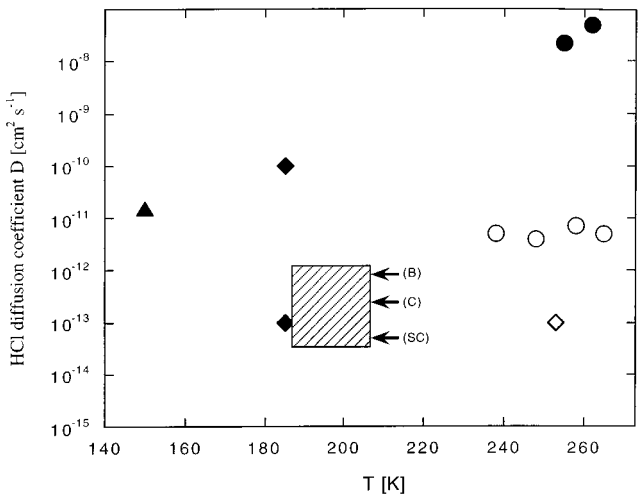


**Figure 13.** Comparison of the diffusion coefficient $D_{HCl}$ [$cm^2\ s^{-1}$] in ice measured in this work (hatched area) with literature values: (○) Thibert and Dominé (1997);[30] (◆) Wolff et al. (1989);[34] (●) Krishnan and Salomon (1969);[49] (◇) Wolff et al. (1989);[34] (▲) Horn and Sully (1997).[35]

topography [45,46] indirectly yielded $H_2O$ self-diffusion coefficients ranging from $D = 1.8 \times 10^{-13}$ $cm^2\ s^{-1}$ to $D = 6.8 \times 10^{-12}$ $cm^2\ s^{-1}$ for $T = 221-252$ K. The correlation between the isotopic tracer and X-ray topographical measurements strongly argues for an interstitial diffusion mechanism. More recently, Livingston et al.[15] investigated the diffusion of HDO into ultrathin single-crystal $H_2{}^{16}O$ ice multilayers ($d \leq 100$ nm) using the laser-induced thermal desorption (LITD) technique. They measured $D = 2.2 \times 10^{-16}$ to $3.9 \times 10^{-14}$ $cm^2\ s^{-1}$ at $T = 153-170$ K and derived an activation energy of $E_A = 17$ kcal/mol and a preexponential factor of $D_0 = 4.2 \times 10^8$ $cm^2\ s^{-1}$. The values of $D_{H_2O}$ on ultrathin films of thickness $<1$ $\mu$m are larger by a factor of approximately 150 than those obtained on macroscopic ices which could be attributed to surface-induced perturbations leading to a "quasi-liquid" $H_2O$ layer on ice. Extrapolations to stratospheric temperatures led to $D_{H_2O}$ ranging from $1.5 \times 10^{-15}$ to $9.6 \times 10^{-13}$ $cm^2\ s^{-1}$ at 180 K to $D_{H_2O} = 4 \times 10^{-13}$ to $8.6 \times 10^{-10}$ $cm^2\ s^{-1}$ at 210 K.[15] NMR investigations[14] of the self-diffusion of $H_2O$ on small ice particles at $T = 253-273$ K indicate that the self-diffusion coefficient in the "quasi-liquid" layer is about 2 orders of magnitude larger than that in single-crystal bulk ice, with an activation energy of $E_A = 5.6$ kcal/mol.

## Conclusion

In this work, we have presented an indirect way to measure the molecular diffusion coefficient $D$ in a solid frozen sample. Despite the fact that $D$ has been obtained indirectly in the present experiments by interrogating the gas phase only, the values we obtain are commensurate with those deduced from other techniques. We note that our method is highly sensitive to the ice morphology and avoids any artifact due to the influence of the substrate on the interface which may be the case for optical measurements on ice films thinner than 1 $\mu$m. RPEs are generally applicable, whereas dope and probe experiments require a rapid probe reaction such as R-1. It is not surprising that both RPEs, which measure the kinetics of loss from the gas phase, and dope and probe experiments measure consistent results of $F_L$ because the rate-controlling step is in both cases the interface-to-bulk loss process, whose time scale is much longer than the residence time in the reactor. RPEs highlight bulk loss processes of gas-phase species on ice, characterized by the surface-to-bulk flux $F_L$, whose value depends on the type of ice as well as on the gas. $F_L(D_2O)$ strongly depends on the substrate, with a value of $(4 \pm 3) \times 10^{14}$ molecule $cm^{-2}\ s^{-1}$ on bulk (B) ice which is roughly 2 orders of magnitude larger than that for single-crystal (SC) ice at 190 K ($F_L = (6 \pm 3) \times 10^{12}$ molecule $cm^{-2}\ s^{-1}$). The substrate dependence in the case of HCl was much less pronounced, perhaps because the measured values are getting close to the limit of the experimental sensitivity of $5 \times 10^{11}$ molecule $cm^{-2}\ s^{-1}$. The rate law seems to be first order in HCl in the region below $10^{15}$ molecules per pulse and becomes zero order for higher HCl partial pressure. This transition may be due to the "liquid" nature of the ice surface,[12] inducing an artifact caused by the limiting value of the evaporation rate occurring at doses where the HCl/ice interface becomes liquidlike. The temperature dependence of $F_L(HCl)$ and $F_L(H_2O)$ displays a positive activation energy $E_A = 3.0 \pm 0.5$ and $5.3 \pm 0.7$ kcal/mol, respectively. Such values are consistent with those concerning $H_2O$ self-diffusion, as observed for instance on small ice particles with an activation energy $E_A = 5.6$ kcal/mol,[14] but are significantly smaller than other values reported in the literature.[45,46,50] This shows the large influence of the type of ice on the activation parameters for $H_2O$ self-diffusion.

The dope and probe experiments have confirmed the feasibility of the measurement as well as the value of $F_L$ obtained in RPEs. They revealed additional structural properties of the ice, namely, the presence of a thin interface where HCl is located and thus immediately available for bimolecular reactions. The thickness $h$ of the interfacial region was found to depend on the ice preparation: $h \approx 100$ nm for single-crystal ice at 190 K, $h \approx 200$ nm for condensed ice, and $h \approx 1000$ nm were found for bulk ice. The trend in $h$ with respect to the type of samples can be correlated with increasing structural defects in the ice, such as grain boundaries and dislocations, which certainly occur in higher numbers in polycrystalline ice compared to single-crystal ice at this length scale. However, one has to take into account an uncertainty of a factor of 2 for $h$.

The diffusion coefficient $D_{HCl}$ in ice could be derived from the value of $F_L(HCl)$. $D_{HCl}$ was found to be in the range of $3 \times 10^{-14}$ to $1.5 \times 10^{-12}$ $cm^2\ s^{-1}$ at 190 K on macroscopic ice samples, which is comparable to the values of Thibert and Dominé,[30] who found $D_{HCl}$ to be $5 \times 10^{-12}$ $cm^2\ s^{-1}$ in the temperature range of $-35$ to $-8$ °C. $D_{H_2O}$ was estimated to be 2 orders of magnitude larger than $D_{HCl}$ at 200 K, which comes close to the value of the self-diffusion coefficient of $H_2O$ in macroscopic polycrystalline ice ($10^{-10}$ $cm^2\ s^{-1}$ at 200 K[36]). $F_L$ for HBr is smaller by a factor of 5 compared to the value for HCl, which may be an indication that the diffusion coefficient of HBr in ice is lower than that of HCl. As pointed out by Barnaal and Slotfeldt-Ellingsen,[47] this may be due to its larger ionic radius and lower mobility compared to HCl.

Our vapor-deposited ice samples of thickness of a few micrometers are representative of the frozen particles encountered in the atmosphere. HCl seems to be located in a region near the surface at the extent of less than $h = 1$ $\mu$m. From our present results, the HCl partitioning into ice particles such as cirrus clouds and PSC (II) and its further availability for heterogeneous reactions according to R-1 and R-2 may depend on the size distribution of the particles as well as on their lifetime. For particles of mean radius $h$, reaction R-1 would be the main process occurring during their lifetime, giving rise to a $Cl_2$ production which would depend on the amount of HCl adsorbed on the particle. On the other hand, for particles of mean radius larger than $h$, such as for PSC (II) particles,[48]

hydrolysis, reaction R-2, may compete with reaction R-1 once the near-surface region has been sufficiently depleted.

**Acknowledgment.** We acknowledge generous funding from the AVINA Foundation supporting the Alliance for Global Sustainability within the project Regional Air Quality and Global Climate Change. The work was also supported by a grant from OFES in the framework of the EU-sponsored project Environment and Climate, subproject COBRA.

## References and Notes

(1) Solomon, S. M.; Garcia, R. R.; Rowland, F. S.; Wuebbles, D. J. *Nature* **1986**, *321*, 755.
(2) Farman, J. C.; Gardiner, B. G.; Shanklin, J. D. *Nature* **1985**, *315*, 207.
(3) Zondlo, M. A.; Barone, S. B.; Tolbert, M. A. *J. Phys. Chem. A* **1998**, *102*, 5735.
(4) Hanson, D. R.; Ravishankara, A. R. *J. Geophys. Res.* **1991**, *96*, 5081.
(5) Leu, M.-T.; Keyser, L. F.; Timonen, R. S. *J. Phys. Chem. B* **1997**, *101*, 6259.
(6) McCoustra, M. R. S.; Horn, A. B. *Chem. Soc. Rev.* **1995**, *23*, 195.
(7) Donsig, H. A.; Vickerman, J. C. *Faraday Discuss.* **1995**, *100*, 348.
(8) Donsig, H. A.; Herridge, D.; Vickerman, J. C. *J. Phys. Chem. A* **1998**, *102*, 2302.
(9) Caloz, F.; Fenter, F. F.; Rossi, M. J. *J. Phys. Chem.* **1996**, *100*, 7494.
(10) Knight, C. A. *J. Glaciol.* **1996**, *42*, 585.
(11) Chaix, L.; van den Bergh, H.; Rossi, M. J. *J. Phys. Chem. A* **1998**, *102*, 10300.
(12) Flückiger, B.; Thielmann, A.; Gutzwiller, L.; Rossi, M. J. *Ber. Bunsen-Ges. Phys. Chem.* **1998**, *102*, 915.
(13) Flückiger, B. Ph.D. Thesis N*o*. 2158, Ecole Polytechnique Fédérale de Lausanne, Lausanne, Switzerland, 2000.
(14) Mizuno, Y.; Hanafusa, N. *J. Phys. Cl* **1987**, *48*, 511.
(15) Livingston, F. E.; Whipple, G. C.; George, S. M. *J. Phys. Chem. B* **1997**, *101*, 6127.
(16) Caloz, F.; Fenter, F. F.; Tabor, K. D.; Rossi, M. J. *Rev. Sci. Instrum.* **1997**, *68*, 3172.
(17) Leu, M.-T. *Geophys. Res. Lett.* **1988**, *15*, 17.
(18) Hanson, D. R.; Ravishankara, A. R. *J. Phys. Chem.* **1992b**, *96*, 2682.
(19) Chu, L. T.; Leu, M.-T.; Keyser, L. F. *J. Phys. Chem.* **1993**, *97*, 12798.
(20) Wooldridge, P. J.; Zhang, R.; Molina, M. J. *J. Geophys. Res.* **1995**, *100*, 1389.
(21) Zhang, R.; Leu, M.-T.; Keyser, L. F. *J. Phys. Chem.* **1994a**, *98*, 13563.
(22) Molina, M. In *The Chemistry of the Atmosphere*: *its impact on Global Change*; Blackwell, J. G., Ed.; Oxford, U.K., 1994.
(23) Worsnop, D. R.; Fox, L. E.; Zahniser, M. S.; Wofsy, St. C. *Science* **1993**, *259*, 71.
(24) Tabazadeh, A.; Turco, R. P.; Drdla, K.; Jacobson, M. Z.; Toon, O. B. *Geophys. Res. Lett.* **1994**, *21*, 1619.
(25) Hanson, D. R.; Ravishankara, A. R. *J. Phys. Chem.* **1994**, *98*, 5728.
(26) Hanson, D. R. *Geophys. Res. Lett.* **1992a**, *19*, 2063.
(27) Molina, M. J.; Tso, T. L.; Molina, L. T.; Wang, F. C. Y. *Science* **1987**, *238*, 1253.
(28) Wofsy, S. C.; Molina, M. J.; Salawitch, R. J.; Fox, L. E.; McElroy, M. B. *J. Geophys. Res*. **1988**, *93*, 2442.
(29) Hanson, M.; Mauersberger, K. *J. Phys. Chem.* **1990**, *94*, 4700.
(30) Thibert, E.; Dominé, F. *J. Phys. Chem. B* **1997**, *101*, 3554.
(31) Eisenberg, D.; Kauzmann, W. *The Structure and Properties of Water*; Oxford University Press: New York, 1969.
(32) Huber, H.; Jaccard, C.; Roulet, M. *Physics and Chemistry of Ice*; Royal Society of Canada: Ottawa, Canada, 1973.
(33) Graeme, E. M.; Nowick, A. S. *Diffusion in Crystalline Solids*; Academic Press: Orlando, FL, 1984.
(34) Wolff, E. W.; Mulvaney, R.; Oates, K. *Geophys. Res. Lett*. **1989**, *16*, 487.
(35) Horn, A. B.; Sully, J. *J. Chem. Soc., Faraday Trans.* **1997**, *93*(*16*), 2741.
(36) Livingston, F. E.; Whipple, G. C.; George, S. M. *J. Chem. Phys.* **1998**, *108* (*5*), 2197.
(37) Dengel, O.; Riehl, N. *Phys. Kondens. Mater*. **1963**, *1*, 191.
(38) Kuhn, W.; Thürkauf, M. *Helv. Chim. Acta* **1958**, *41*, 938.
(39) Itagaki, J. *J. Phys. Soc. Jpn.* **1964**, *19*, 1081.
(40) Itagaki, J. *J. Phys. Soc. Jpn.* **1967**, *22*, 427.
(41) Blicks, H.; Dengel, O.; Riehl, N. *Phys. Kondens. Mater*. **1966**, *4*, 375.
(42) Delibaltas, P.; Dengel, O.; Helmreich, D.; Riehl, N.; Simon, H. *Phys. Kondens. Mater*. **1966**, *5*, 166.
(43) Ramseier, R. O. *J. Appl. Phys*. **1967**, *38*, 2553.
(44) For a comprehensive classical review of the chemical physics of ice, see: Hobbs, P. V. *Ice Physics*; Clarendon Press: Oxford, 1974.
(45) Goto, K.; Hondoh, T.; Higashi, A. *Jpn. J. Appl. Phys*. **1986**, *25*, 351.
(46) Hondoh, T.; Goto, A.; Hoshi, R.; Ono, T.; Anzai, H.; Kawase, R.; Pimienta, P.; Mae, S. *Rev. Sci. Instrum.* **1989**, *60*, 2494.
(47) Barnaal, D.; Slotfeldt-Ellingsen, D. *J. Phys. Chem.* **1983**, *87*, 4321.
(48) Turco, R. P.; Toon, O. B.; Hamill, P. *J. Geophys. Res.* **1989**, *94*, 16493.
(49) Krishnan, P. N.; Salomon, R. E. *J. Phys. Chem.* **1969**, *73*(*8*), 2680.
(50) Brown, D. E.; George, S. M. *J. Phys. Chem.* **1996**, *100*, 15460.